DYNAMICS OF EXCITED ATOMS AND MOLECULES INTERACTING WITH EXTERNAL FIELDS

Sigrid Ina Simonsen

Dissertation for the degree of Philosophiae Doctor (PhD)

Department of Physics and Technology
University of Bergen

June 2013

SCIENTIFIC ENVIRONMENT

The work presented in this thesis has been supervised by Professor Jan Petter Hansen at the Department of Physics and Technology at the University of Bergen. Co-supervisors have been Professor Morten Førre and Professor Ladislav Kocbach at the same institute. The PhD-candidate and supervisors are members of the group of Optics and Atomic Physics at the University of Bergen. The PhD work has been a part of the reseach project "Dynamics of Rydberg Atoms, Molecules and Matter", financed by The Research Council Norway (Frinatek project no. 804647) . The candidate has participated in the ongoing Nordforsk Network “Time-domain quantum processes studied by ultrafast radiation pulses” and in the Nordita workshop “Studying Quantum Mechanics in the Time Domain”.

ACKNOWLEDGEMENTS

My supervisor Prof. Jan Petter Hansen deserves the first and foremost thanks in this acknowledgement. Your positivism, enthusiasm and encouragement have been the foundations for the the whole project, and I have learned a lot from you. Much appreciation to Prof. Morten Førre and Prof. Ladislav Kocbach for always keeping an open door, and for contributing to my scientific enlightenment. I have had fantastic years at the group of Optics and Atomic Physics at the University of Bergen, and would like to thank every colleague, former and present, for this.

To my office-mates throughout the last five years, Stian, Sigurd, Ingjald, Arne and Aleksander. I owe you a lot for arranging an office spot for me during my first years at UiB, and I will never forget the many joys and frustrations that we have shared. And not to forget, the vast amount of bread. We may not be colleagues in the future, but we will always be friends.

I am greatful to Prof. Pablo Fainstein at Centro Atómico Bariloche for facilitating our stay in Argentina, and Daniel and Juan for making life outside work very pleasant. Thank you on behalf of myself and my family. We hope to visit you again someday. Prof. Alain Dubois at Université Pierre et Marie Curie in Paris also deserves thanks for welcoming me there, and of course Stéphane and Nicolas for their help and patience.

The thesis would not have been if not for my colleagues, but I could not have finished it without the daily support of Kristian and Edvard. You are the loves of my life. To old friends and new friends, Marit and Joy-Loi, Maria and Magnhild in particular, thank you for all good times that have been and will be. You always make me see the world from new perspectives, which indeed is very useful in this profession, but most of all help keep me sane. My sisters, Ingeborg and Ragnhild, and the rest of my family, thank you for being the best cheerleading troop ever. I feel really privileged that you are my family.

And finally, thanks to my parents, who taught us the joy of learning and experiencing from an early age. This thesis is for you.

ABSTRACT

This thesis is a theoretical study of the behavior of electrons in atoms and molecules subjected to external electromagnetic fields. Three electronic systems have been central in this work, the atomic and quasimolecular Rydberg states and the carbon allotrope graphene. The exaggerated properties of the highly excited Rydberg atoms, such as long lifetime, large spatial extension and low binding energy make them excellent candidates for both theoretical and experimental considerations. The analytical solutions of the hydrogen atom in quantum mechanics provide a good description for most Rydberg atoms. This is exploited in the work presented in this thesis and the accompanying papers, where we show results of numerical computations on interacting Rydberg atoms, with and without the presence of radiating fields, as well as dynamic Rydberg wave packets influenced by a train of femtosecond laser pulses. In the final part of the thesis the optical process of high-order harmonic generation in an extended molecular structure, represented by graphene, is considered.

Rydberg atoms have a large dipole moment due to the large average electronic radius in the atom, which leads to a very strong dipole-dipole coupling between interacting particles in a gas of cold Rydberg atoms. This interaction, which is dependent on the internuclear separation between the atoms, induces a shift in the energy levels, which again prohibits the excitation of more than one atom in the gas, an effect commonly known as the *Rydberg blockade*. A correlated behavior is observed for the *intrashell* transitions in mutually excited Rydberg atoms. The microwave field driven dynamics is significantly supressed for internuclear distances below a given conditional radius which scales linearly with the principal quantum number n. Such an entangled electronic behavior may open for the realization of quantum gates applied in quantum informatics.

The long-range interaction of Rydberg atoms is dominated by the dipole-dipole terms. Nevertheless, the investigation of two interacting Rydberg atoms, without the influence of electromagnetic radiation, has shown that the lower order multipolar terms play a vital role in the energy shifts as well as for the electronic probability distributions. We found that the energy curves, when including all multipole orders, correspond to both repulsive and attractive states with a stronger repulsion than attraction. We also propose a laser assisted approach for stabilization of Rydberg gases by controlled transitions between such attractive and repulsive energy states.

Single-electron ionization of a dynamic Rydberg wave packet confined within a single energy level has been investigated. The ionization probability of an intrashell Rydberg wave packet depends strongly on the degree of polarization. For a wave packet driven repeatedly between the circular (least polarized) state and the linear (most polarized) state by a rotating microwave field and subjected to a train of femtosecond laser

pulses, the ionization probability will depend crucially on the laser repetition rate and number of pulses. The angular-resolved ionization probability and energy distribution in the continuum are also influenced by these parameters.

The last part of the thesis is devoted to the study of high-order harmonic generation (HHG) in graphene. In the simple man's model HHG can be described by an electron that is ionized and driven in an external field, after which it returns to the parent atom and recombines, emitting a high-energy photon with frequency that is a multiple of the incident laser frequency. We show that the harmonic spectra obtained from the interaction with linearly as well as circularly polarized femtosecond lasers yield harmonics up the classical limit for extended molecules. In contrast to diatomic molecules, the stable grid structure of graphene ensures that the harmonic generation cutoff remains constant with increasing signal power as the graphene diameter extends beyond the classical limit. Additionally, for circularly polarized lasers harmonics exceeding the classical predictions have been observed.

LIST OF PUBLICATIONS

The thesis is based on the following publications:

I L. Sælen, S. I. Simonsen and J. P. Hansen, *Interatom intrashell blockade*, Physical Review A **83**, 015401 (2011)

II S. I. Simonsen, L. Kocbach and J. P. Hansen, *Long-range interactions and state characteristics of interacting Rydberg atoms*, Journal of Physics B **44**, 165001 (2011)

III S. I. Simonsen, S. A. Sørngård, M. Førre and J. P. Hansen, *Femtosecond-pulse-train ionization of Rydberg wave packets*, Physical Review A **86**, 043423 (2012)

IV S. A. Sørngård, S. I. Simonsen and J. P. Hansen, *High-order harmonic generation from graphene: Strong attosecond pulses with arbitrary polarization*, Physical Review A **87**, 053803 (2013)

V S. I. Simonsen, S. A. Sørngård, M. Førre and J. P. Hansen, *High-order harmonic generation in graphene flakes exposed to circularly polarized femtosecond pulses*, submitted to Journal of Physics B, May 2013

List of Abbreviations

GTO Gaussian type orbitals

HHG High-order harmonic generation

HOMO Highest occupied molecular orbital

SFA Strong-field approximation

SPM Stationary phase method

TDSE Time-dependent Schrödinger equation

TISE Time-independent Schrödinger equation

CONTENTS

LIST OF FIGURES

CHAPTER 1

INTRODUCTION

Throughout the entire human history there have been groundbreaking discoveries that have altered our perceptions of nature and forced new thinking. The current year we celebrate the 100-years anniversary for such a mind changing idea in the field of atomic physics. When the Danish physicist Niels Bohr in 1913 published the atomic model bearing his name, it marked the start of a scientific and technological revolution that has prevailed to this day. In the *Bohr model* the atom is described as a small, positively charged nucleus surrounded by negatively charged electrons orbiting in circularly shaped, classical trajectories with well-defined energy values [1]. The classical model reigning at the time described the electronic motion by Maxwell's theory of electromagnetism, but had a fundamental problem; It predicted that all atoms would loose energy in the form of electromagnetic radiation, and consequently the electron would spiral inwards until it eventually collapsed into the nucleus. Not only did Bohr's innovative idea that the electron motion is restricted to discrete energies explain why atoms are stable, it also provided a solution to one of the most essential problems of the time, the explanation of the spectral lines from atoms. As early as 1888 Johannes Rydberg was able to describe the spectral lines in hydrogenlike atoms with the formula [2],

$$\frac{1}{\lambda_{\text{vac}}} = RZ^2\left(\frac{1}{n_1^2} - \frac{1}{n_2^2}\right), \tag{1.1}$$

where λ_{vac} is the wavelength of electromagnetic radiation in vacuum, Z is the atomic number and $n_1 < n_2$ are integers. The fundamental constant $R \approx 1.097 \times 10^7\,\text{m}^{-1}$ became known as the Rydberg constant. Despite scientific consensus on the validity of the Rydberg formula, it lacked a theoretical foundation. The main success of the Bohr atomic model lay in its ability to provide a long awaited explanation of the Rydberg formula, both qualitatively and quantitatively. The masterwork of Niels Bohr put him in the front along with the leading physicists at the time, despite his young age. Lord Rutherford, whose work Bohr built his upon, even stated,

> *"Bohr's original quantum theory of spectra was one of the most revolutionary, I suppose, that was ever given to science, and I do not know of any theory that has been more successful. I consider the work of Bohr one of the greatest triumphs of the human mind."*

The first decades of the 20th century were very productive ones in regards to the development of the quantum theory. The perhaps most famous equation in quantum

mechanics was put forward in 1926 by Erwin Schrödinger. We know it simply as the time-dependent Schrödinger equation [3–5], given by

$$\mathrm{i}\frac{\partial}{\partial t}\Psi = H\Psi, \tag{1.2}$$

where Ψ is the wavefunction and H is the Hamiltonian operator representing the total energy of the system. In the standard interpretation of quantum mechanics, also known as the *Copenhagen interpretation*, formulated by Bohr and his assistant Werner Heisenberg in Copenhagen during the years 1924-1927, all physical properties of the quantum mechanical system is fully characterized by the wavefunction which depends on the spatial coordinates and time. The Schrödinger equation (1.2) describes the time evolution of the wavefunction, which is essentially probabilistic, in the sense that the absolute square of the wavefunction provides the spatial probability distribution of the quantum system. However, any measurements made cannot have results that violate Heisenberg's uncertainty relations, i.e., $\Delta_i\Delta_j \geq \hbar/2$, where Δ_i and Δ_j represent the standard deviations of two complementary physical properties, for example position x and momentum p.

It is no exaggeration to say that the emergence of the quantum theory, and with that the improved understanding of atoms and molecules, has had a profound impact on the world as we know it. From basic science to our daily lives, the possibility to control and influence atomic systems has played a vital role in the technological revolution we have seen the last hundred years. In fact, it is hard to come up with areas that are totally unaffected by technologies based on fundamental quantum mechanics. Personal computers and mobile phones have almost become a necessity to take part in the modern society. Today, nearly 90 percent of the world's population have their own cell phone, a situation it is hard to believe even the most visionary could have anticipated a century ago.

The realization of the *laser* around 1960 is one of the most important applications of quantum theory to a real system [6, 7]. The laser is an acronym for *light amplification by stimulated emission of radiation* and the theoretical foundations date all the way back to the work of Albert Einstein in 1917 [8]. A laser takes direct advantage of the quantization of electron energy in atoms and molecules. The light emitted is coherent, enabling it to be concentrated on very tiny spots or over large distances. Lasers have a wide selection of applications, from common office laser printers to eye surgery, measurement devices for detecting speed or range, entertainment and military purposes. Since the very beginning of laser research, a variety of specialized laser types has been developed and optimized to meet different criteria and goals. The first lasers had an output power of some thousand watts and a duration of a few millisecond (10^{-3} s). Nowadays, scientists have been able to produce laser systems with an output power of petawatts (10^{15} W), which is more than a thousand times the power consumed by the USA in any instant of time. Such high-intensity lasers are currently being exploited in scientific explorations of laser ignited nuclear fusion processes for future energy production [9, 10].

From a scientific point of view the laser is perhaps the most powerful tool in the study of the interactions between light and matter. The widely tunable dye laser, discovered independently by Peter P. Sorokin in USA and Fritz P. Schäfer in Germany in 1966 [11, 12], made it possible to excite atoms into well-defined high-energy states,

also known as *Rydberg states* [13], opening a new era in atomic physics with the manipulation and study of such systems.

Today, isolated Rydberg atoms can be experimentally prepared in almost any linear combination of states and substates [14–16]. In a gas of Rydberg atoms, it has been shown that the large dipole moment of the Rydberg states induces a detuning which prohibits the interacting particles to become optically excited simultaneously. This entanglement, known as the Rydberg dipole blockade [17, 18], has been proposed as a way to implement controllable quantum bits for the realization of quantum computers [19].

In 1961, shortly after the invention of the laser, Peter Franken and colleagues at the University of Michigan demonstrated what is known as frequency doubling, or second harmonic generation [20]. They sent a ruby laser beam with wavelength of 694 nm into a quartz sample, and recorded an output light with wavelength of 347 nm, half the wavelength and twice the frequency of the incident field. This was the first demonstration of the nonlinear optical process of harmonic generation, and in the following decades scientists were able to produce harmonics of higher and higher order [21–23]. The properties of the generated light, such as temporal and spatial coherence, strongly depend on the driving laser. In addition, neighboring harmonics can add constructively to form a high-intensity pulse of very short duration. For a femtosecond (10^{-15} s) laser with wavelength of 800 nm, the output pulse can then be in the attosecond (10^{-18} s) regime [24, 25], which is the typical timescale for electronic motion in atoms and molecules. Visualizing the motion of these electrons thus requires a spatial resolution at the Ångström[1] scale and a temporal resolution at the attosecond scale, which has previously not been possible. Nowadays, powerful laser systems are available as table top devices. Thus high-order harmonic generation has proved an efficient way to produce coherent XUV/Soft X-ray pulses on the attosecond timescale, with a wide range of applications such as ultrafast photoemission spectroscopy and ultrahigh resolution imaging [26, 27].

The motivation behind this thesis is to study the behavior of electrons in atoms and molecules influenced by other atoms in the presence of external electromagnetic fields. The thesis can be divided into three main parts, based on the accompanying papers; The first part (Paper I and II) deals with the dynamics between two interacting Rydberg atoms. The second part (Paper III) investigates the influence of a femtosecond laser pulse on a dynamic wave packet of a single Rydberg atom. The third, and last, part (Paper IV and V) is devoted to the study of laser-matter interactions in an extended molecular system, more specifically the generation of high-order harmonics in a sheet of graphene from the interaction with a femtosecond laser pulse. In the three following chapters an overview of the basic theory on which the papers have been built is presented, including a description of Rydberg atoms, the Stark effect, the strong-field approximation and high-order harmonic generation, followed by a summary and a brief outlook. The last chapter gives an introduction to the five papers enclosed in the dissertation.

Throughout the thesis and the papers atomic units, where m_e, $\hbar$ and e are scaled to unity, have been used unless stated otherwise. An additional list of derived units is

[1] An Ångström is a unit length equal to 10^{-10} m. It is named after Anders Jonas Ångström, a Swedish physicist who, despite his relatively short life, made significant contributions to the fields of spectroscopy and astrophysics during the 19th century.

given in Appendix A.

CHAPTER 2

RYDBERG ATOMS

An atom with one or more electrons excited to an energy level of high principal quantum number n is said to be in a Rydberg state. Any chemical element can be excited into a Rydberg atom, and given that the excited electron is far enough from the ionic core, the atom can be treated similar to a hydrogen atom. This makes Rydberg atoms particularly convenient for theoretical computations, seeing that the hydrogen atom is one of the few quantum mechanical systems with analytical solutions. However, the screened nuclear potential arising from the presence of the remaining electrons surrounding the nucleus may induce quantum defects in the Rydberg state energy as compared to the hydrogen energy levels. Rydberg atoms have a very large mean radius and correspondingly low binding energy, which causes them to be easily perturbed by even weak fields. However, the average lifetime of such excited states scales as $n^{4.5}$ [28], and hence undisturbed Rydberg atoms are far more reluctant to decay than lower excited states. Rydberg atoms also possess a very large dipole moment, which particularly influences the interplay between these particles in a cold gas. The combination of these exaggerated properties makes Rydberg atoms especially well-suited for linking experimental results and theory.

2.1 The Schrödinger equation

As mentioned in the introductory chapter, all physical properties of a quantum mechanical system are described by its wavefunction $\Psi(\mathbf{r},t)$. The evolvement of the wavefunction in time is governed by the *time-dependent Schrödinger equation* (TDSE), which for a one-particle system reads,

$$\mathrm{i}\frac{\partial}{\partial t}\Psi(\mathbf{r},t) = \left(-\frac{\nabla^2}{2} + V(\mathbf{r},t)\right)\Psi(\mathbf{r},t), \tag{2.1}$$

where the terms in the brackets make up the Hamilton operator, consisting of a kinetic energy term to the left and a time-dependent potential $V(\mathbf{r},t)$ to the right. The Hamilton operator is Hermitian, meaning that its eigenvalues are real and that the eigenvectors form a complete orthonormal basis. When all potentials influencing the quantum system are included in the Hamiltonian, the solutions of the TDSE yield all the information there is to know about the system. However, in most cases, the TDSE cannot

be solved exactly, and approximations must be made in order to obtain satisfactory solutions. One such approach is *perturbation theory*, which applies for atoms subjected to "small" disturbances. Perturbation theory is described in Sec. 3.2.2 and in Sec. 3.3 for time-dependent and time-independent electromagnetic fields, respectively. However, when the interfering field is strong, perturbative approximations are no longer valid. An alternative approach may then be to treat the system within the *strong-field approximation* [29–31]. This will be considered in the theory for high-order harmonic generation in Ch. 4.

2.1.1 Time-independent potential

When describing the wavefunction of a Rydberg atom, we make the assumption that the electron in the Rydberg state is sufficiently far from the nucleus so that we can employ the solutions of the hydrogen atom. Since the hydrogenic Coulomb potential ($V(\mathbf{r}) = -1/r$) is time-independent, we can separate the time-dependency from the solutions of the TDSE in Eq. (2.1). The *stationary states* thus take the form $\Psi(\mathbf{r},t) = \psi(\mathbf{r})\mathrm{e}^{-\mathrm{i}Et}$, where E is the energy and $\psi(\mathbf{r})$ satisfies the *time-independent Schrödinger equation* (TISE), which for the hydrogen atom reads,

$$\left(-\frac{\nabla^2}{2} - \frac{1}{r}\right)\psi(\mathbf{r}) = H_0\psi(\mathbf{r}) = E\,\psi(\mathbf{r}). \tag{2.2}$$

The wavefunction $\psi(\mathbf{r})$ can be separated in spherical coordinates into a radial function and spherical harmonics as,

$$\psi_{nlm}(\mathbf{r}) = R_{nl}(r)Y_{lm}(\theta,\phi), \tag{2.3}$$

depending on the principal, angular and magnetic quantum numbers denoted n, l and m, respectively.

The corresponding energy eigenvalues obtained from Eq. (2.2) are given by [32]

$$E_n = -\frac{1}{2n^2}. \tag{2.4}$$

The electronic probability density can be obtained by the wavefunction squared, $|\psi(\mathbf{r})|^2 = \psi^*(\mathbf{r})\psi(\mathbf{r})$. Since the states $\psi(\mathbf{r})$ form a complete, orthonormal set of functions, we can expand any (normalized) wavefunction $\Psi(\mathbf{r},t)$ in them such that

$$\Psi(\mathbf{r},t) = \sum_i c_i(t)\psi_i(\mathbf{r}). \tag{2.5}$$

where $c_i(t)$ is the expansion coefficients for state $\psi_i(\mathbf{r})$. Due to the orthonormality, we obtain the following expression for the probability distribution,

$$|\Psi(\mathbf{r},t)|^2 = \sum_i |c_i(t)|^2, \tag{2.6}$$

and therefore the coefficients $c_i(t)$ are commonly known as the probability amplitudes.

2.1.2 Parabolic coordinates

The one-electron TISE (2.2) is separable in spherical coordinates for any spherically symmetric potential $V(\mathbf{r})$. Yet, when the potential is the Coulomb potential, the problem is separable also in parabolic coordinates. In addition, such a choice of coordinates turns out to be beneficial when the atom is influenced by an external electric field, such as in the Stark effect (see Sec. 3.3). Despite the fact that the spherical symmetry of the potential $V(\mathbf{r})$ is lost in the Stark effect, the Schrödinger equation in parabolic coordinates remains separable even in the presence of the static field [28, 33]. The relations between parabolic coordinates (ξ,η,ϕ) and Cartesian coordinates (x,y,z) read,

$$\begin{aligned} x &= \sqrt{\xi\eta}\cos\phi \\ y &= \sqrt{\xi\eta}\sin\phi \\ z &= \frac{1}{2}(\xi-\eta) \end{aligned} \tag{2.7}$$

with $\xi,\eta\in[0,\infty]$ and $\phi\in[0,2\pi]$. Omitting the steps in the derivations, the normalized bound wavefunction of hydrogenic atoms in parabolic coordinates reads [32],

$$\begin{aligned} \psi_{n_1n_2m}(\xi,\eta,\phi) &= \frac{\sqrt{2}}{n^2}\sqrt{\frac{n_1!n_2!}{[(n_1+|m|)!(n_2+|m|)!]^3}} \\ &\quad\times \mathrm{e}^{-(\rho_1+\rho_2)/2}(\rho_1\rho_2)^{|m|/2}L^{|m|}_{n_1+|m|}(\rho_1)L^{|m|}_{n_2+|m|}(\rho_2)\frac{\mathrm{e}^{\mathrm{i}m\phi}}{\sqrt{2\pi}} \end{aligned} \tag{2.8}$$

where $\rho_1=\xi/n$, $\rho_2=\eta/n$. The principal and magnetic quantum numbers are related to the parabolic quantum numbers n_1 and n_2 such that $n_1+n_2=n-|m|-1$.

2.2 Interacting Rydberg atoms

The constant interplay between Rydberg atoms in gas phase can cause collisions resulting in ionization and heating, and as such it constitutes a great challenge for experimentalists [34]. On the other hand, these interactions also provide a unique insight into the processes governing them, and might as such open for the control of interacting Rydberg atoms [35, 36]. In Paper II the long-range interaction between two neutral hydrogen atoms, both excited to the same energy level, is examined. The nuclei A and B are separated a distance R, directed along the z axis, cf. Fig. 2.1, with the associated electronic coordinates $\mathbf{r}_{1,2}$.

The Hamiltonian for the system thus reads,

$$\begin{aligned} H &= \sum_{i=1,2} H_0(\mathbf{r}_i) + \frac{1}{R} - \frac{1}{|\mathbf{r}_1-\mathbf{R}|} - \frac{1}{|\mathbf{r}_2+\mathbf{R}|} + \frac{1}{|\mathbf{r}_1-\mathbf{r}_2-\mathbf{R}|} \\ &= \sum_{i=1,2} H_0(\mathbf{r}_i) + V(\mathbf{r}_1,\mathbf{r}_2,\mathbf{R}) \end{aligned} \tag{2.9}$$

where H_0 is the Hamiltonian for the isolated hydrogen atoms, cf. Eq. (2.2). In the present case we consider solely large internuclear distances, and consequently the in-

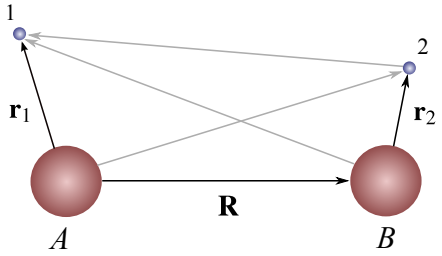

Figure 2.1: Coordinate system describing the interaction between two Rydberg atoms separated by the internuclear vector $\mathbf{R}$ parallel to the z axis.

teraction term $V(\mathbf{r}_1,\mathbf{r}_2,\mathbf{R})$ can be expressed asymptotically as [37],

$$V(\mathbf{r}_1,\mathbf{r}_2,\mathbf{R}) \approx \sum_{l_1=1}^{\infty}\sum_{l_2=1}^{\infty} \frac{V_{l_1,l_2}(\mathbf{r}_1,\mathbf{r}_2)}{R^{l_1+l_2+1}}. \tag{2.10}$$

The function $V_{l_1,l_2}(\mathbf{r}_1,\mathbf{r}_2)$ is simply a sum over products of the spherical harmonics $Y_{lm}(\theta,\phi)$ for each atom, see Paper II and references therein. The total wavefunction of the system can be expanded in products of the eigenstates ψ_{nlm} assigned to each atom, with $n_1 = n_2 = n$, by

$$\Psi(\mathbf{r}_1,\mathbf{r}_2) = \sum_{\substack{l_1,l_2=0 \\ m_1,m_2=-l_1,-l_2}}^{\substack{m_1,m_2=l_1,l_2 \\ l_1,l_2=n-1}} c_{l_1m_1,l_2m_2}\psi_{nl_1m_1}(\mathbf{r}_1)\psi_{nl_2m_2}(\mathbf{r}_2). \tag{2.11}$$

The alignment of the internuclear axis with the z axis restricts the perturbation to only the product states with $m_1 + m_2 = 0$, the so-called Σ states. For a two-atom system mutually excited to the $n = 2$ level there are six Σ states. By exploiting symmetry properties, like invariance to particle exchange and reflection by the xy plane, we can make linear combinations of the six basis states, so that the matrix representing the long-range interaction becomes block diagonal,

$$V^{\mathrm{sym}}(R) = \begin{pmatrix} 0 & -\frac{18}{R^3} & 0 & -\sqrt{2}\frac{9}{R^3} & 0 & 0 \\ -\frac{18}{R^3} & \frac{864}{R^5} & -\sqrt{2}\frac{108}{R^4} & \sqrt{2}\frac{432}{R^5} & 0 & 0 \\ 0 & -\sqrt{2}\frac{108}{R^4} & \frac{18}{R^3} & -\frac{108}{R^4} & 0 & 0 \\ -\sqrt{2}\frac{9}{R^3} & \sqrt{2}\frac{432}{R^5} & -\frac{108}{R^4} & \frac{432}{R^5} & 0 & 0 \\ 0 & 0 & 0 & 0 & -\frac{18}{R^3} & 0 \\ 0 & 0 & 0 & 0 & 0 & 0 \end{pmatrix}. \tag{2.12}$$

The dipole-dipole terms (R^{-3}) dominate, but as seen in the bottom panel of Fig. 2.2 the lower order terms play a vital role for smaller internuclear separations. In these plots the zero energy level has been adjusted to $-1/2n^2$. The energy curves are non-symmetrically distributed around the adjusted $E = 0$ level, in contrast to the plot in the upper panel, which shows that when only the dipole terms are included, the energy curves are symmetrically distributed around $E = 0$. The electronic density plots in the

insets show that also the wavefunction is strongly influenced by the multipolar terms in the interaction, with a heavy accumulation towards the molecular center for the highest energy state when including all orders of the interaction term. However, when only the dipole terms are considered the wavefunction is symmetrically distributed around each nuclei. Interestingly, the asymmetry in the electronic distribution remains even for large R, i.e., in the regions where the energy curves are very well given by the dipole terms alone.

In the last section of Paper II we propose a mechanism to prevent the process of unwanted heating in cold Rydberg gases. By having a set of masers operating at frequencies resonant to the energy separations one could drive transitions between the attractive and repulsive energy states and thereby cool the system.

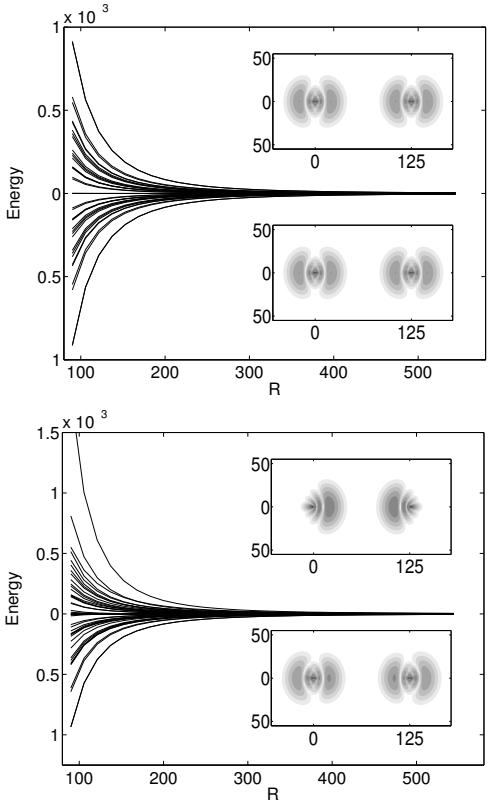

Figure 2.2: Top panel: Potential energy curves resulting only from the dipole-dipole interaction terms for the Σ states of two Rydberg atoms mutually excited to the $n = 4$ manifold, plotted as a function of the internuclear distance R. The zero energy level has been adjusted to $-1/2n^2$. Bottom panel: The potential energy curves for the same system of Rydberg atoms as in the top panel, except here all multipole orders of the interaction are included. The upper (lower) inset in both panels shows the electronic probability density at $R = 125$ a.u. for the highest (lowest) energy state. The figure was published in Paper II.

CHAPTER 3

RYDBERG ATOMS IN WEAK ELECTROMAGNETIC FIELDS

Treating the interaction between an atom and an external electromagnetic field in quantum electrodynamics requires the electromagnetic field to be described in terms of each photon in the field. However, in the papers enclosed in this thesis, the photon density is high enough for the photons to be treated as a continuous variable, which justifies the use of the *semi-classical* approach. That is to say, we describe the external electromagnetic field classically by Maxwell's equations, while the atomic system is treated quantum mechanically. Furthermore, we assume that the nucleus has infinite mass, and that only the electrons are affected by the radiation field, i.e., we ignore the interaction between the nucleus and the external field.

3.1 The electromagnetic field

In classical electrodynamics the electric and magnetic fields are described by two vectors, $\mathbf{E}(\mathbf{r},t)$ and $\mathbf{B}(\mathbf{r},t)$, satisfying Maxwell's equations, which can be derived from the scalar and vector potentials $\phi(\mathbf{r},t)$ and $\mathbf{A}(\mathbf{r},t)$ by

$$\mathbf{E}(\mathbf{r},t) = -\nabla\phi(\mathbf{r},t) - \frac{\partial}{\partial t}\mathbf{A}(\mathbf{r},t), \tag{3.1}$$

and

$$\mathbf{B}(\mathbf{r},t) = \nabla \times \mathbf{A}(\mathbf{r},t). \tag{3.2}$$

The fields $\mathbf{E}$ and $\mathbf{B}$ remain unchanged under the gauge transformation $\mathbf{A} \to \mathbf{A} + \nabla\chi$ and $\phi \to \phi - \partial\chi/\partial t$, where $\chi = \chi(\mathbf{r},t)$ is a real, differentiable function, and thus we are free to impose the convenient *Coulomb gauge* on the field vector, i.e. $\nabla \cdot \mathbf{A} = 0$. In addition, since there are no sources present in the field, $\phi = 0$, and $\mathbf{A}(\mathbf{r},t)$ satisfies the wave equation

$$\nabla^2\mathbf{A}(\mathbf{r},t) - \frac{1}{c^2}\frac{\partial}{\partial t}\mathbf{A}(\mathbf{r},t) = 0, \tag{3.3}$$

with plane wave solutions that can be written as

$$\mathbf{A}(\mathbf{r},t) = A_0(\omega)\cos(\mathbf{k}\cdot\mathbf{r} - \omega t + \varphi)\hat{\varepsilon}, \tag{3.4}$$

where $\mathbf{k}$ is the wave vector, φ denotes the phase and $\hat{\varepsilon}$ is the polarization unit vector.

3.1.1 The dipole approximation

The electronic wavefunction of a ground state atom typically extends over a few Ångström. For interactions with radiation of low frequency and corresponding long wavelength, we can therefore usually ignore the spatial variation of the field over the atom. In other words we assume that $|\mathbf{k}\cdot\mathbf{r}| \ll 1$. This is known as the *dipole approximation*, and for a laser it is generally said to be valid as long as $r \ll 137/\omega$. The zeroth order expansion of the vector potential describing the field thus becomes,

$$\mathbf{A}(\mathbf{r},t) = A_0(\omega)\cos(\mathbf{k}\cdot\mathbf{r}+\omega t+\varphi)\hat{\varepsilon} \approx A_0(\omega)\cos(\omega t+\varphi)\hat{\varepsilon}. \tag{3.5}$$

In the dipole approximation $\mathbf{A}(t)$, and hence $\mathbf{E}(t)$, are functions depending only on the time, and consequently the magnetic field $\mathbf{B}(\mathbf{r},t)$ vanishes, cf. Eq. (3.2). This leads to the following relation between the electric field and the vector potential,

$$\mathbf{E}(t) = -\frac{\mathrm{d}\mathbf{A}(t)}{\mathrm{d}t}. \tag{3.6}$$

When the extent of the atom is large, such as Rydberg atoms of very high principal quantum number n, or the frequency of the field is very high, the validity of the dipole approximation must be assessed. In Paper III we study the photoionization processes of a Rydberg atom interacting with a train of femtosecond pulses. The Rydberg atom is initially in the energy level corresponding to $n = 16$, and seeing that the orbital radius scales as n^2, the radius $r \approx 2.5\times10^2$ a.u. Compared to the incident 800 nm femtosecond laser ($\omega = 0.057$ a.u.), which leads to $137/\omega \approx 2.5\times10^3$ a.u., we conclude that r is sufficiently small for the system to be treated within the dipole approximation.

3.2 One-electron atoms in external fields

The time-dependent Schrödinger equation (TDSE) for the hydrogen atom in an external electromagnetic field reads,

$$\mathrm{i}\frac{\partial}{\partial t}\Psi(\mathbf{r},t) = (H_0 + H_{\mathrm{int}})\Psi(\mathbf{r},t), \tag{3.7}$$

where $\mathbf{r}$ is the coordinate of the electron and H_0 is the field-free Hamiltonian given in Eq. (2.2). The term

$$H_{\mathrm{int}}(t) = \mathbf{A}(t)\cdot\mathbf{p} + \frac{1}{2}\mathbf{A}^2(t) = -\mathrm{i}\mathbf{A}(t)\cdot\boldsymbol{\nabla} + \frac{1}{2}\mathbf{A}^2(t) \tag{3.8}$$

describes the interaction of the electron with the external radiation field in the Coulomb gauge. Here we have inserted the substitution $\mathbf{p} = -\mathrm{i}\boldsymbol{\nabla}$ for the momentum operator.

3.2.1 Gauge transformations

The TDSE in Eq. (3.7) is said to be in the *velocity gauge* due to the interaction term which couples the vector field $\mathbf{A}(t)$ and the momentum operator $\mathbf{p}$. By performing the following gauge transformation on the wavefunction

$$\Psi^{\mathrm{L}}(\mathbf{r},t) = \mathrm{e}^{\mathrm{i}\mathbf{A}(t)\cdot\mathbf{r}}\Psi(\mathbf{r},t), \tag{3.9}$$

and substituting into Eq. (3.7), we obtain the Schrödinger equation in the *length gauge*

$$\mathrm{i}\frac{\partial}{\partial t}\Psi^{\mathrm{L}}(\mathbf{r},t) = (H_0 + \mathbf{E}(t)\cdot\mathbf{r})\Psi^{\mathrm{L}}(\mathbf{r},t). \tag{3.10}$$

The label refers to the interaction of the atom with the radiating field being described by the electric field $\mathbf{E}(t)$ and the position $\mathbf{r}$. If no further approximations are made, matrix elements and expectation values calculated in the different gauges must yield identical results.

3.2.2 Time-dependent perturbation theory

In the case of weak fields, the time-dependent Hamiltonian $H_{\mathrm{int}} = \mathbf{E}(t)\cdot\mathbf{r} \equiv H'$ can be treated as a small perturbation. The eigenvalues and corresponding normalized eigenstates of the unperturbed part H_0 are given by $H_0\psi_k = E_k\psi_k$. The solutions of the TDSE in Eq. (3.7) can be expanded in the complete basis of the known stationary states as,

$$\Psi(\mathbf{r},t) = \sum_k c_k(t)\psi_k(\mathbf{r})\mathrm{e}^{-\mathrm{i}E_k t} \tag{3.11}$$

where the expansion coefficients $c_k(t)$ satisfy the coupled equations given by,

$$\frac{\mathrm{d}c_n(t)}{\mathrm{d}t} = -\mathrm{i}\sum_k H'_{nk}(t)c_k(t)\mathrm{e}^{\mathrm{i}\omega_{nk}t}. \tag{3.12}$$

The coupling matrix elements are given by $H'_{nk} = \langle\psi_n|H'(t)|\psi_k\rangle$ and $\omega_{nk} = (E_n - E_k)$.

For a system initially in the well-defined bound state ψ_a interacting with a laser pulse turned on at time $t = 0$, the first-order transition amplitudes are given by,

$$c_b(t) = -\mathrm{i}\int_0^t \langle\psi_b|\mathbf{E}(t')\cdot\mathbf{r}|\psi_a\rangle\mathrm{e}^{\mathrm{i}\omega_{ba}t'}\mathrm{d}t'. \tag{3.13}$$

These amplitudes can be used to evaluate transitions within the bound states, i.e., excitation processes, as well as transitions from bound states to the continuum, i.e., ionization processes. In Paper III the latter scenario is considered for a Rydberg wave packet interacting with a train of femtosecond laser pulses. The transition amplitudes are employed in the evaluation of the total ionization probability, in addition to the angular resolved ionization probability and energy distribution in the continuum.

3.3 The linear Stark effect

The *Stark effect* refers to the splitting of the energy levels in an atom or molecule due to the presence of an external static electric field. We here assume that the electric field strength E_0 is low enough for allowing the system to be treated by time-dependent perturbation theory, but at the same time large enough for fine structure effects to be disregarded. For hydrogen in the first excited state ($n = 2$) this means that $10^5\,\mathrm{V/m} \ll E_0 \ll 10^{10}\,\mathrm{V/m}$.

The perturbation due to an electric field directed along the z axis which is uniform throughout the atom is given by the Hamiltonian,

$$H' = E_0 z. \tag{3.14}$$

According to perturbation theory we need to calculate the dipole matrix elements given by,

$$\langle \psi_{nlm}|H'|\psi_{n'l'm'}\rangle = E_0\langle \psi_{nlm}|z|\psi_{n'l'm'}\rangle \tag{3.15}$$

The selection rules for the angular integrals predict that these matrix elements vanish unless $m = m'$ and $l = l' \pm 1$.

As mentioned in Sec. 2.1.2 the TDSE for a one-electron atom represented in parabolic coordinates remains separable even in the presence of a constant electric field. We therefore adopt such coordinates in our description of the Stark effect. With the Hamiltonian (3.14) in parabolic coordinates reading,

$$H' = \frac{1}{2}E_0(\xi - \eta), \tag{3.16}$$

and the hydrogenic parabolic wavefunction in Eq. (2.8), the first-order correction to the energy of the unperturbed atom reads,

$$E^{(1)} = \pm\frac{3}{2}E_0 n(n_1 - n_2) = \pm\frac{3}{2}E_0 nk. \tag{3.17}$$

The energy depends on n and the difference between the parabolic quantum numbers n_1 and n_2, and this is commonly known as the Stark quantum number $k \equiv n_1 - n_2$. The highest energy is obtained when $n_1 = n-1$ and $n_2 = 0$, and the lowest energy when n_1 and n_2 are interchanged, which leads to $|k_{\max}| = (n-1)$. The hydrogenic parabolic wavefunction can be expanded in the spherical wavefunctions by Clebsch-Gordan coefficients by the following relation [13],

$$|\psi_{nkm}\rangle = \sum_l (-1)^l \left\langle \frac{n-1}{2}, \frac{m-k}{2}, \frac{n-1}{2}, \frac{m+k}{2} \middle| lm \right\rangle |\psi_{nlm}\rangle. \tag{3.18}$$

Figure 3.1 shows an illustration of the linear Stark effect in a hydrogen atom in the $n = 8$ level.

The two most polarized Stark states (with $|km\rangle = |\pm k_{\max}, 0\rangle$) have an energy correction of approximately $\pm 3E_0 n^2/2$. To avoid crossing between adjacent energy levels with energy spacings of $1/n^3$, we must have that $3E_0 n^2/2 \ll 1/n^3$. This gives the *Inglis-Teller limit* for the electric field strength [38],

$$E_0 = \frac{1}{3}n^5, \tag{3.19}$$

for the avoided crossing of the energy levels in the Stark effect.

3.4 Rydberg atom in a weak electromagnetic field

When external time-dependent fields are applied to a Rydberg atom, its states are altered according to the field strength and variation in time. For a constant, low intensity electric field the Rydberg n-level can split in equidistant sublevels, due to the linear Stark effect. If an additional oscillating field is applied, slowly varying in time and with photon energy low enough such that excitation between n-levels or ionization is

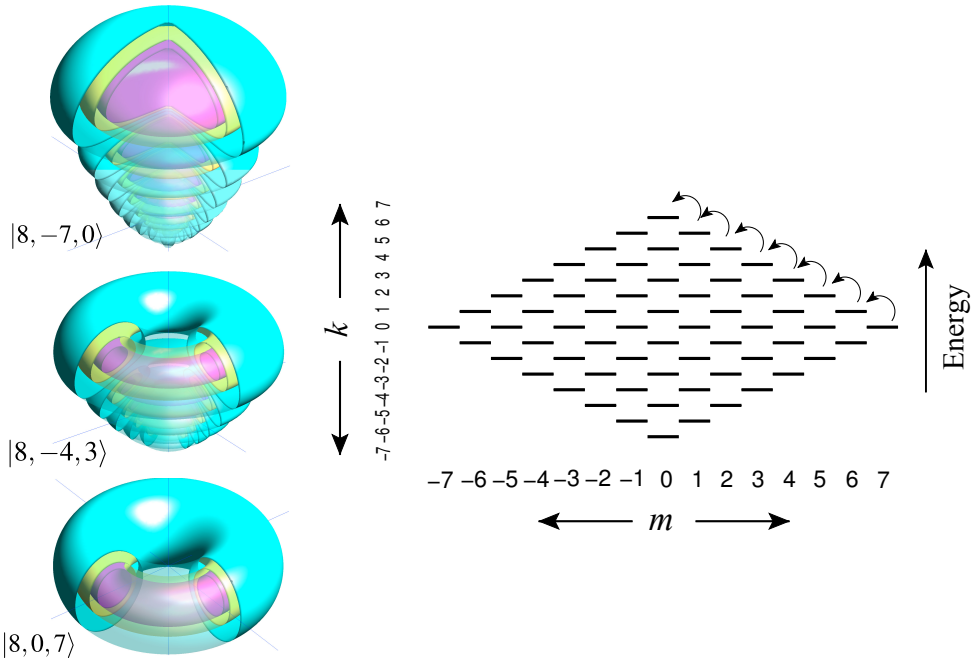

Figure 3.1: Stark states $|nkm\rangle$ of a Rydberg atom in the $n = 8$ level due to the static electric field E_z. The states populated by the resonant microwave field in the xy plane, from the initial circular state ($|nkm\rangle = |8,0,7\rangle$) to the most polarized state ($|nkm\rangle = |8,7,0\rangle$), are indicated by arrows.

prohibited, the entrapped Rydberg wave packet can undergo transitions within the manifold, provided the frequency of the external field is in resonance with the Stark splitting [14, 15, 39, 40], see Fig. 3.1. It follows that the oscillating field frequency must be $\omega_0 = \frac{3}{2}nE_0 \ll 1/n^3$.

A general treatment of the intrashell time-evolution of Rydberg atoms in external electric and magnetic field, $\mathbf{E}(t)$ and $\mathbf{B}(t)$, can be formulated in the following manner [41–43]. When the electron transitions are restricted to a single n manifold, the position operator $\mathbf{r}$ can be substituted by the Pauli operator replacement $-\frac{3}{2}n\mathbf{a}$, where $\mathbf{a}$ is the quantum mechanical counterpart of the classical Runge-Lenz vector $\mathbf{L}$, defined as

$$\mathbf{a} = \sqrt{\frac{1}{-2E}}\left[\frac{1}{2}(\mathbf{p}\times\mathbf{L} - \mathbf{L}\times\mathbf{p}) - \frac{\mathbf{r}}{r}\right]. \tag{3.20}$$

The dynamics can be described in terms of the pseudospins

$$\mathbf{J}_\pm = \frac{1}{2}(\mathbf{L} \pm \mathbf{a}), \tag{3.21}$$

for which the contribution to the Hamiltonian from the weak fields becomes

$$H_{\text{int}} = \boldsymbol{\omega}_+ \cdot \boldsymbol{J}_+ + \boldsymbol{\omega}_- \cdot \boldsymbol{J}_-, \tag{3.22}$$

with $\boldsymbol{\omega}_\pm = \frac{1}{2}\mathbf{B} \pm \frac{3}{2}\mathbf{E}$. Here we have redefined the zero energy level to that of $-1/2n^2$. The two independent spins $\mathbf{J}_\pm$ play the role of angular momentum operators "rotating" in the effective magnetic fields $\boldsymbol{\omega}_\pm$. They have eigenvalues $\mathbf{J}_\pm^2|j_\pm, m_\pm\rangle = j(j+1)|j_\pm, m_\pm\rangle$ where $j = (n-1)/2$, and the eigenenergies of the Hamiltonian become

$$E = m_+|\boldsymbol{\omega}_+| + m_-|\boldsymbol{\omega}_-|, \tag{3.23}$$

with $m_\pm = -(n-1)/2, -(n-1)/2+1, \ldots, (n-1)/2-1, (n-1)/2$. Based on the Majorana principle of spin reduction from 1932, which proves that a system with total spin J rotating in a field can be replaced by $2J$ spin $1/2$ systems in the same field [44], Kazansky and Ostrovsky demonstrated in 1996 that the solution of the Schrödinger equation with the Hamiltonian (3.22) could be separated into two spin $1/2$ systems [45]. Consequently, $\mathbf{J}_\pm = \sum_{i=1}^{2J} \mathbf{j}_i$, which greatly reduces the complexity of the problem, and we are left with solutions of the form,

$$|jm\rangle = c_{-1/2}(t)\left|\frac{1}{2}, -\frac{1}{2}\right\rangle + c_{+1/2}(t)\left|\frac{1}{2}, \frac{1}{2}\right\rangle, \tag{3.24}$$

where the coefficients satisfy the coupled differential equations,

$$\mathrm{i}\frac{\mathrm{d}}{\mathrm{d}t}\begin{pmatrix} c_{-1/2} \\ c_{1/2} \end{pmatrix} = \frac{1}{2}\begin{pmatrix} -\omega_z^\pm & \omega_x^\pm + \mathrm{i}\omega_y^\pm \\ \omega_x^\pm - \mathrm{i}\omega_y^\pm & \omega_z^\pm \end{pmatrix}\begin{pmatrix} c_{-1/2} \\ c_{1/2} \end{pmatrix}. \tag{3.25}$$

This method applies for any n level, and for a given initial condition the system (3.25) is usually straightforward to evaluate numerically. In Paper I and III the intrashell dynamics of Rydberg atoms is derived using this method, considering only the presence of an electric field.

3.4.1 Rydberg blockade

The strong dipole-dipole interaction between Rydberg atoms can induce a shift in the energy levels of the Rydberg states. Consequently, in a gas of cold atoms, the Rydberg excitation of one atom becomes dependent on the excitation of the other atoms. This is the mechanism behind the so-called *Rydberg blockade* effect [18, 46, 47]. It can be described by a system of two atoms initially in the ground state, with the two-atom state denoted $|g,g\rangle$. The principles of this excitation scheme is shown in Fig. 3.3. For independent atoms an external field with a resonant frequency ω can excite the atoms to the state $|e,g\rangle$ or $|g,e\rangle$ and further to $|e,e\rangle$. However, for non-independent atoms, the intermediate state is given by $\left(1/\sqrt{2}\left(|e,g\rangle \pm |g,e\rangle\right)\right)$, and the strong dipole-dipole interaction in the doubly excited state $|e,e\rangle$ will shift the energy level by $\Delta E = \pm C/R^3$, as described in Sec. 2.2. For sufficiently small internuclear distance R, this shift becomes so large that the field is no longer in resonance with the energy splitting, and hence the system is prohibited to excite more than one atom.

3.4.2 Interacting Rydberg atoms in a weak field

When two Rydberg atoms mutually excited to the same energy level are placed in a crossed electromagnetic field that comply to the criteria for intrashell dynamics, the

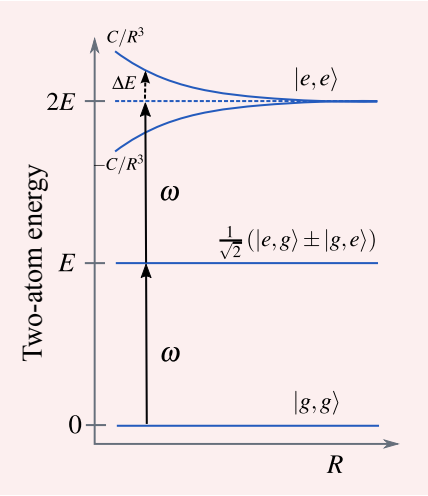

Figure 3.2: Rydberg dipole blockade between two atoms separated a distance R. The ground state $|g\rangle$ is coupled to the excited state $|e\rangle$ by the resonant frequency ω. The dipole-dipole interaction arising when both atoms are in the excited state, i.e. the two-atom system $|e,e\rangle$, induces an energy shift $\Delta E = \pm C/R^3$. When this shift becomes large enough the external field is no longer in resonance with the energy splitting, and the system is locked in the intermediate state $\left(1/\sqrt{2}\left(|e,g\rangle \pm |g,e\rangle\right)\right)$, which corresponds to only one atom being excited.

dipole interaction can cause the states to become entangled and the intrashell behavior to become dependent in analogy to the Rydberg blockade mechanism.

A system of two interacting Rydberg atoms separated by $\mathbf{R} = [0,0,R]$ can be described by the Hamiltonian

$$H = \sum_{i=1,2} H_0(\mathbf{r}_i) + V(\mathbf{r}_1, \mathbf{r}_2, \mathbf{R}), \tag{3.26}$$

where $H_0(\mathbf{r}_i)$ is the field-free Hamiltonian. We consider only the dipole-dipole terms in the interaction $V(\mathbf{r}_1, \mathbf{r}_2, \mathbf{R})$ described by Eq. (2.10). The crossed-field setup comprises a constant electric field along the z direction, and a rotating microwave field in the xy plane written as

$$\mathbf{E}(t) = [\varepsilon_0 \cos \omega t, \varepsilon_0 \sin \omega t, E_z], \tag{3.27}$$

which drives the intrashell transitions. When the internuclear separation is large, the Rydberg atoms are driven from the initial circular state to the most polarized (linear) state, and back again during the time $T_{\text{rev}} = 4\pi/3n\varepsilon_0$, with close to unit probability, as seen by the full black curve in Fig. 3.3. However, for diminishing internuclear distances the probability for revival of the initial state decreases until the initial state becomes completely locked, plotted by red (gray) lines in the figure. The electrons are thus prohibited from leaving the initial state, and the intrashell dynamics is blocked.

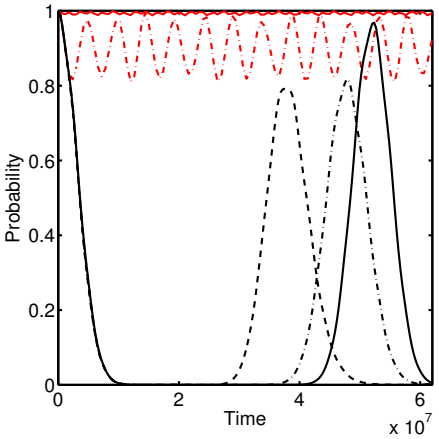

Figure 3.3: Time development (in a.u.) of the initial circular state of two interacting Rydberg atoms in the principal $n = 8$ level with internuclear distance R (in a.u.). The external electric field is of the form $\mathbf{E} = [\varepsilon_0 \cos \omega t, \varepsilon_0 \sin \omega t, E_z]$. Full black line, $R = 5000$; Dashed-dot black line, $R = 3000$; Dashed black line, $R = 2000$; Dashed-dot red (gray) line, $R = 800$; Full red (gray) line, $R = 600$. Figure published in Paper I.

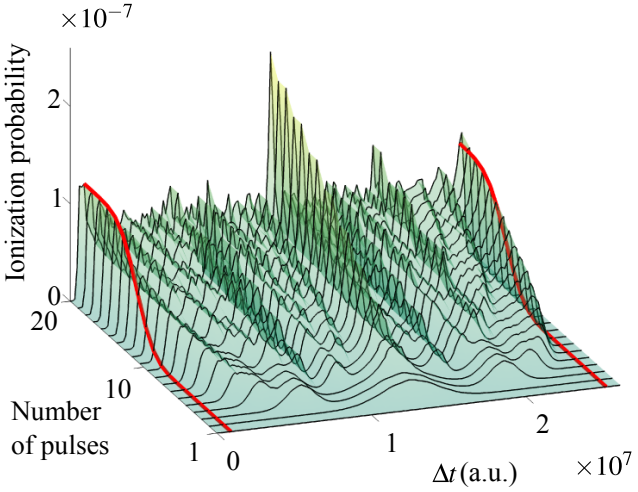

Figure 3.4: Ionization probability for a Rydberg wave packet ($n = 16$) driven in a Stark setup hit by a train of femtosecond laser pulses. N is the number of succeeding pulses and Δt is the time delay. The initial state is the circular Stark state $|nkm\rangle = |16, 0, 15\rangle$. The plot was published in Paper III.

3.4.3 Pulse-train ionization of a Rydberg wave packet

In Paper III we consider the ionization process of an intrashell Rydberg wave packet, for a single atom in the energy level of principal quantum number $n = 16$, from the interaction with a train of femtosecond laser pulses. The wave packet is initially in the circular Stark state ($|nkm\rangle = |16, 0, 15\rangle$) and is driven in a Stark setup by a resonant microwave field, via transitions similar to the ones shown in Fig. 3.1 for the $n = 8$ level. That is to say, the wave packet drifts repeatedly between the circular state and the linear state. The strong dependency of the ionization probability on the Stark quantum number k leads to large variations in the total ionization probability when varying the number of succeeding femtosecond pulses N and the time separation Δt between the pulses, as shown in Fig. 3.4. We see that certain combinations of N and Δt yield a strong increase or suppression in the ionization probability.

CHAPTER 4

HIGH-ORDER HARMONIC GENERATION

Atoms and molecules subjected to intense laser pulses can produce photons with frequencies that are multiples of the central frequency ω_0 of the incident light. The process is known as high-order harmonic generation (HHG), and can be described classically by the simple man's model, also called the three-step model, after the three main steps in the process [48]: The irradiated atom undergoes tunneling ionization and releases an electron to the continuum. The electron is then accelerated in the field during half an optical cycle of the laser pulse, after which it returns to the ion and recombines while emitting a high-energy photon with a frequency that is N times the central frequency ω_0 of the driving laser field. If the system consists of a monochromatic field interacting with an atom or a homonuclear molecule, the harmonic order N of the outgoing photon is restricted to take on odd values only, i.e. the output frequency is,

$$\Omega = N\omega_0, \quad \text{where} \quad N = 1,3,5,\ldots. \tag{4.1}$$

In this thesis the interaction of atoms and molecules with high-intensity lasers is described within the strong-field approximation (SFA) [29–31]. A summary of this method is given in the following section of this chapter, after which the process of HHG is considered, with emphasis on HHG in graphene, which is the subject for Paper IV and V.

4.1 Strong-field approximation

The strong-field approximation is built upon three basic assumptions:

- Firstly, in the strong-field regime we must have $U_\mathrm{p} > I_\mathrm{p}$. In other words the *ponderomotive energy* U_p, defined as the classical quivering energy of a free electron in the field, given by

  $$U_\mathrm{p} = \frac{E_0^2}{4\omega_0^2}, \tag{4.2}$$

  must exceed the binding energy of the atom, I_p. This allows us to assume that the continuum part of the wavefunction is not influenced by the Coulomb potential, $V(r)$.

- Secondly, the bound wavefunction is described by a single state only. This is a valid assumption as long as the binding energy is much larger than the photon

energy of the incident field, $I_p/\omega_0 \gg 1$. Thus the mixing of the bound states can be neglected.

- Thirdly, we assume that only a small fraction of the bound wavefunction is ionized, so we need not worry about depletion of the initial state. This approximation is similar to the one made in time-dependent perturbation theory, described in Sec. 3.2.2. However, it should be emphasized that SFA is considered a non-perturbative method.

4.1.1 Volkov states in length gauge and velocity gauge

The TDSE for a free electron with momentum $\mathbf{p}$ in an external laser field, described in the dipole approximation by the vector potential $\mathbf{A}(t)$, reads

$$\mathrm{i}\frac{\partial}{\partial t}\Psi^{\mathrm{V}}(\mathbf{r},t) = \frac{1}{2}\left[\mathbf{p}+\mathbf{A}(t)\right]^2\Psi^{\mathrm{V}}(\mathbf{r},t). \tag{4.3}$$

The solutions are the *velocity gauge Volkov states*, given by

$$\Psi^{\mathrm{V}}(\mathbf{r},t) = \frac{1}{(2\pi)^{3/2}}\mathrm{e}^{\mathrm{i}\mathbf{k}\cdot\mathbf{r}-\mathrm{i}S(k,t,t_0)}, \tag{4.4}$$

where $\mathbf{k}$ is the wave vector, and the function $S(k,t,t_0) = \frac{1}{2}\int_{t_0}^{t} dt' \left[\mathbf{k}+\mathbf{A}(t')\right]^2$ can be interpreted as the classical effect of the field on the electron.

By performing the gauge transformation on the wavefunction, cf. Eq. (3.9), we obtain the TDSE for a free electron in the field in the length gauge,

$$\mathrm{i}\frac{\partial}{\partial t}\Psi^{\mathrm{L}}(\mathbf{r},t) = \left[\frac{\mathbf{p}^2}{2}+\mathbf{E}(t)\cdot\mathbf{r}\right]\Psi^{\mathrm{L}}(\mathbf{r},t), \tag{4.5}$$

with the *length gauge Volkov states* given by

$$\Psi^{\mathrm{L}}(\mathbf{r},t) = \frac{1}{(2\pi)^{3/2}}\mathrm{e}^{\mathrm{i}[\mathbf{k}+\mathbf{A}(t)]\cdot\mathbf{r}-\mathrm{i}S(k,t,t_0)}. \tag{4.6}$$

4.1.2 The SFA wavefunction

In accordance with the third assumption made above the SFA wavefunction can be written as a sum over the bound and the continuum part,

$$\Psi(\mathbf{r},t)^{\mathrm{SFA}} \simeq \Psi_{\mathrm{b}}(\mathbf{r},t) + \int \mathrm{d}^3k\, c(\mathbf{k},t)\Psi_{\mathrm{c}}(\mathbf{r},t). \tag{4.7}$$

The amplitudes for ionization from the bound state to a Volkov state in the continuum are given by

$$c(\mathbf{k},t) = -\mathrm{i}\int_0^t \mathrm{d}t' \langle\Psi_{\mathrm{c}}(\mathbf{r},t')|V(\mathbf{r},t')|\Psi_{\mathrm{b}}(\mathbf{r},t')\rangle, \tag{4.8}$$

where $V(\mathbf{r},t)$ denotes the time-dependent interaction potential, given by $\mathbf{E}(t)\cdot\mathbf{r}$ in the length gauge, and $\mathbf{A}(t)\cdot\mathbf{p}+\mathbf{A}^2(t)/2$ in the velocity gauge. If we assume that the initial state is the hydrogen ground state, with energy ε_0, written as

$$\Psi_{\mathrm{b}}(\mathbf{r},t) = \psi_0(\mathbf{r})\mathrm{e}^{-i\varepsilon_0(t-t_0)}, \tag{4.9}$$

and that the continuum state is the velocity gauge Volkov wavefunction, Eq. (4.4), by substitution into Eq. (4.7) we obtain the following SFA wavefunction in the velocity gauge,

$$\begin{aligned}\Psi(\mathbf{r},t)^{\mathrm{SFA}} &\simeq \psi_0(\mathbf{r})\mathrm{e}^{-i\varepsilon_0(t-t_0)} - \frac{\mathrm{i}}{(2\pi)^3}\int_0^t \mathrm{d}t'\mathrm{e}^{-i\varepsilon_0(t'-t_0)}\int \mathrm{d}^3k\mathrm{e}^{-\mathrm{i}S(k,t,t')} \\ &\times \int \mathrm{d}^3r'\ \mathrm{e}^{-\mathrm{i}\mathbf{k}\cdot\mathbf{r}'}\left[\mathbf{A}(t')\cdot\mathbf{p} + \frac{\mathbf{A}^2(t')}{2}\right]\psi_0(\mathbf{r}')\ \mathrm{e}^{\mathrm{i}\mathbf{k}\cdot\mathbf{r}}. \end{aligned} \tag{4.10}$$

4.2 The HHG spectrum

The HHG power spectrum along a direction $\mathbf{n}$ can be obtained by taking the Fourier transform of the expectation value of the momentum operator with the velocity gauge wavefunctions, Eq. (4.10), as expressed by the following formula:

$$S_{\mathbf{n}}(\omega) = \left|\mathbf{n}\cdot\int_{-\infty}^{\infty}\mathrm{d}t\ \mathrm{e}^{\mathrm{i}\omega t}\langle\Psi(\mathbf{r},t)^{\mathrm{SFA}}|\mathbf{p}|\Psi(\mathbf{r},t)^{\mathrm{SFA}}\rangle\right|^2 \tag{4.11}$$

The matrix elements for HHG can, alternatively to the momentum form given above, be calculated in the dipole or acceleration form. However, it was demonstrated by Baggesen and Madsen that the momentum form is the one that relates directly to the harmonic field obtained by solving Maxwell's wave equations [49]. They also showed that the dipole and acceleration forms could be obtained from the momentum form by some scaling factors depending on the harmonic frequency ω. In Paper IV and V the dipole velocity form is used throughout. The choice of gauge is motivated by the fact that the length gauge gives rise to an unphysical dependency of the HHG spectrum on the internuclear distances in the molecule [31].

When neglecting couplings amongst the continuum states the expectation value of the momentum operator with the velocity gauge SFA wavefunction thus reads,

$$\begin{aligned}\langle\Psi(\mathbf{r},t)|\mathbf{p}|\Psi(\mathbf{r},t)\rangle^{\mathrm{SFA}} &\simeq -\left(\frac{1}{2\pi}\right)^3\int_0^t \mathrm{d}t'\mathrm{e}^{\mathrm{i}\varepsilon(t-t')}\int \mathrm{d}^3k\mathrm{e}^{-\mathrm{i}S(k,t,t')}\times \\ &\underbrace{\int \mathrm{d}^3r\mathrm{e}^{-\mathrm{i}\mathbf{k}\cdot\mathbf{r}}\left[\mathbf{A}(t')\cdot\mathbf{p}+\frac{\mathbf{A}^2(t')}{2}\right]\psi_0(\mathbf{r})}_{R(\mathbf{k},t')}\underbrace{\int \mathrm{d}^3r\psi_0^*(\mathbf{r})\nabla\mathrm{e}^{\mathrm{i}\mathbf{k}\cdot\mathbf{r}}}_{\mathbf{V}(\mathbf{k},t)} \\ &+ \mathrm{c.c.}\end{aligned} \tag{4.12}$$

The integrals $R(\mathbf{k},t')$ and $\mathbf{V}(\mathbf{k},t)$ represent the amplitudes for ionization at time t' during the laser pulse interaction, and recombination at a later time t.

4.2.1 The cutoff

The harmonic spectra obtained in HHG have some characteristic features. The signal strength drops quickly for the first, lower-order harmonics, after which the signal strength levels out over a range of frequencies. This *plateau* is a series of harmonic peaks of equal power, and it usually ends abruptly with the *cutoff harmonic frequency*. Beyond the cutoff the signal strength rapidly falls off, and as such it is a measure of the

maximum photon energy producible in a HHG setup. The cutoff energy can be calculated classically as the maximum energy that an electron can gain in the electric field. This classical approach, which results in,

$$E_{\max} = I_p + 8U_p, \tag{4.13}$$

has been shown to agree very well with experiments for diatomic systems [50, 51]. From a classical point of view the electron in a diatomic system ionizes at one atom, accelerates in the driving field and recombines with the other atom. On the other hand, in the case of a single atom, the electron's only possibility for recombination is with itself. Hence the harmonic frequencies can solely be generated by an electron that is ionized and accelerated in one direction of the driving field amplitude, until the field changes sign and the electron is accelerated back towards the parent ion and recombines. As a result, the maximum harmonic frequency is limited to [52, 53],

$$E_{\max} = I_p + 3.17U_p. \tag{4.14}$$

In Fig. 4.1 the HHG power spectra obtained for a single atom and a diatomic molecule are shown. The characteristic plateau ending in the classically predicted cutoff frequency is evident.

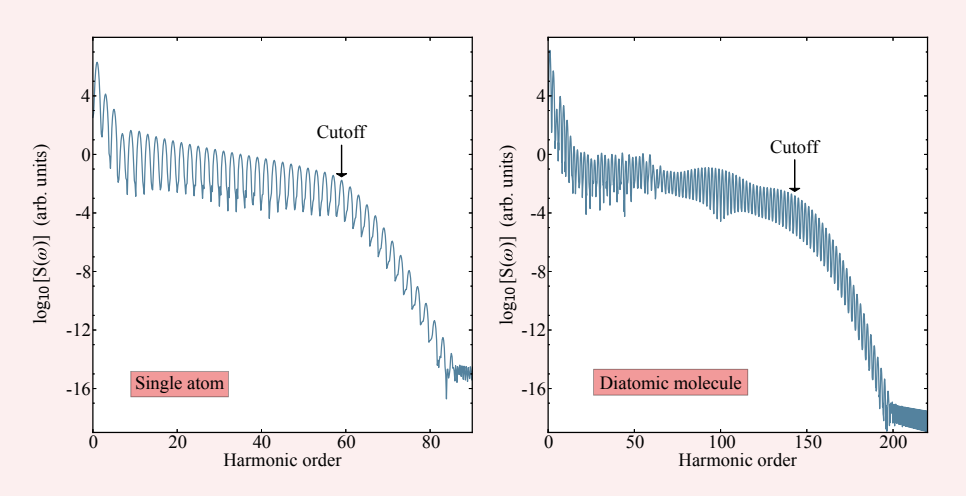

Figure 4.1: HHG power spectrum as function of harmonic order for a linearly polarized laser interacting with a single atom (left panel) and a diatomic molecule (right panel) with internuclear distance $R = 95$ a.u. The classically computed cutoff frequencies for both systems are indicated by arrows. The laser pulse is modeled by a six-cycle plane wave with central frequency $\omega_0 = 0.057$ a.u. (800 nm), and electric field strength $E_0 = 0.114$ a.u. ($I_{\text{peak}} = 4.6 \times 10^{14}\,\text{Wcm}^{-1}$), modulated by a trapezoidal envelope function.

The single atom HHG is also limited to linearly polarized laser fields. Increasing ellipticity on the laser polarization results in a rapidly decreasing harmonic signal for

a single atom, as demonstrated in [54]. These results strongly support the classical picture, which predicts that a higher degree of ellipticity will cause the electron to 'miss' the parent atom during its trajectory in the field. HHG can also be limited by very strong laser fields, with $I_{\text{peak}} \geq 10^{16}\,\text{Wcm}^{-2}$. In such cases the dipole approximation is no longer valid, and the magnetic component of the external field may deflect the electron's trajectory, and ultimately prevent recombination.

4.3 HHG in graphene

Graphene is a monolayer of carbon atoms distributed in a hexagonal pattern, where the carbon atoms are bound together by the strong, but flexible, covalent bonds between hybridized sp^2 orbitals [55]. The extraordinary strength of graphene, combined with very light weight and superior electronic conductivity, give rise to a number of potential applications within electronics and material science, as well as various medical and industrial processes. Hence graphene has received an explosive interest in the last years, and nowadays it is considered a promising material for nonlinear optical processes, such as HHG, in nanostructures [56, 57]. The process of HHG from a flake of graphene is the subject for Paper IV and V.

The chemical and optical properties of graphene is not governed by the sp^2 orbitals, but rather of the highest occupied molecular orbital (HOMO), which in graphene comprises a single p orbital perpendicular to the molecular plane. This allows us to model a graphene layer extended in the xy plane by p_z orbitals distributed on a honeycomb lattice, as illustrated in Fig. 4.2. The bound graphene wavefunction can thus be generated as a linear combination of atomic orbitals by

$$\Psi_{\text{b}}(\mathbf{r},t) = \frac{1}{\sqrt{N}} \sum_{j}^{N} \psi_{\text{b}}(\mathbf{r}_j) \text{e}^{-\text{i}\varepsilon_0(t-t_0)}, \tag{4.15}$$

where each atomic site in the molecule is modeled by a Gaussian type orbital (GTO) of the form,

$$\psi(\mathbf{r}_j) = a_j r_{j_x}^{k_j} r_{j_y}^{l_j} r_{j_z}^{m_j} \text{e}^{-\alpha(\mathbf{r}-\mathbf{R}_j)^2}, \tag{4.16}$$

For p_z we have that $k_j = l_j = 0$ and $m_j = 1$, and ε_0 denotes the HOMO energy eigenvalue. The coefficients and exponents must be carefully evaluated to ensure that the GTOs yield a good approximation to carbon p_z orbitals. In our work they are computed using The General Atomic and Molecular Electronic Structure System (GAMESS), a software package for various chemical computations, including the calculation of molecular orbitals using the Hartree-Fock, or self-consistent field, method [58].

The foremost reason to employ Gaussian functions for calculating molecular orbitals is that the product of two Gaussian functions can be expressed as another Gaussian function, according to the "Gaussian product theorem". Generally this can be described as

$$\text{e}^{-a(k-A)^2} \text{e}^{-b(k-B)^2} = \text{e}^{-\frac{ab}{a+b}(A-B)^2} \text{e}^{-(a+b)(k-P)^2}, \tag{4.17}$$

with $P = (aA + bB)/(a+b)$.

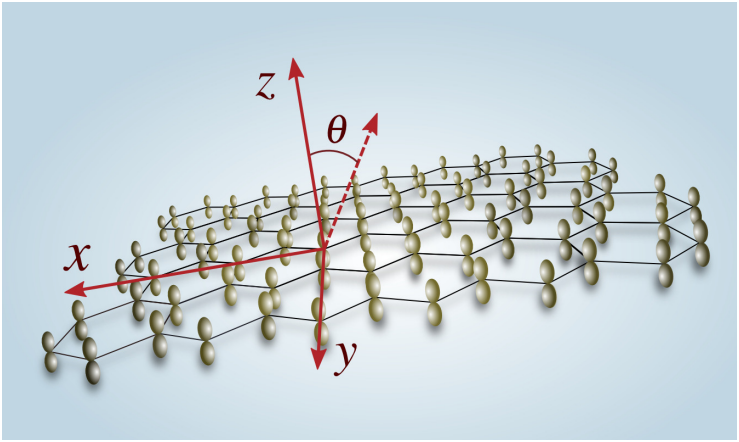

Figure 4.2: Visualization of the graphene sheet, with atomic sites modeled by p_z orbitals distributed on a honeycomb lattice in the xy plane. The angle θ represents the polarization angle of the incident linearly polarized laser light. Figure taken from Paper V.

4.3.1 Evaluation of the integrals

To evaluate the HHG spectra one needs the matrix elements for ionization from the initial state to the Volkov state, and recombination from the Volkov state to the bound state. From Eq. (4.12) we see that in the SFA the process of ionization is expressed by the integral

$$R(\mathbf{k},t') = \int \mathrm{d}^3 r \mathrm{e}^{-\mathrm{i}\mathbf{k}\cdot\mathbf{r}} \left[\mathbf{A}(t')\cdot\mathbf{p} + \frac{\mathbf{A}^2(t')}{2}\right] \psi_\mathrm{b}(\mathbf{r}), \tag{4.18}$$

and for recombination we have that,

$$\mathbf{V}(\mathbf{k},t) = \int \mathrm{d}^3 r \psi_\mathrm{b}^*(\mathbf{r}) \nabla \mathrm{e}^{\mathrm{i}\mathbf{k}\cdot\mathbf{r}}. \tag{4.19}$$

A thing to notice is that the ionization matrix element is a scalar, whereas the recombination matrix element is a vector. Consequently, the components of the driving field in the all polarization directions ($\hat{\varepsilon}_x$,$\hat{\varepsilon}_y$,$\hat{\varepsilon}_z$) will influence the HHG spectrum along a given direction $\mathbf{n}$.

Both matrix elements are analytic functions depending on the electron momentum $\mathbf{k}$. With the graphene wavefunction in Eq. (4.15) as the initial state and by rearranging Eq. (4.12), we obtain the following expectation value,

$$\begin{aligned}\langle\Psi(\mathbf{r},t)|\mathbf{p}|\Psi(\mathbf{r},t)\rangle^{\mathrm{SFA}} \simeq & -\frac{1}{\sqrt{N}}\sum_j^N \left(\frac{1}{2\pi}\right)^3 \int_0^t \mathrm{d}t' \mathrm{e}^{\mathrm{i}\left[\varepsilon_0(t-t') - \frac{1}{2}\int_{t'}^t \mathrm{d}t'' \mathbf{A}^2(t'')\right]} \\ & \times \int \mathrm{d}^3 k \mathbf{V}_j(\mathbf{k},t)\, R_j(\mathbf{k},t')\, \mathrm{e}^{-\mathrm{i}\left[\frac{1}{2}k^2(t-t') + \tilde{\mathbf{A}}\cdot\mathbf{k}\right]} + \mathrm{c.c.},\end{aligned} \tag{4.20}$$

where $\tilde{\mathbf{A}}(t) \equiv \int_{t'}^t \mathrm{d}t'' \mathbf{A}(t'')$. The momentum integrals, $\int \mathrm{d}^3 k$, can either be calculated approximately by applying the stationary phase method (SPM) or by analytic evaluations.

4.3.2 Stationary phase method

The SPM, also known as the saddle-point approximation, is a useful way of approximating integrals of rapidly oscillating functions. For integrals of the form

$$\int_{-\infty}^{\infty} f(x)\mathrm{e}^{\mathrm{i}g(x)}\mathrm{d}x, \tag{4.21}$$

where $f(x)$ is slowly varying and $g(x)$ is rapidly varying, most of the contributions to the integral come from the points where $g'(x)=0$. The points x_s satisfying this criterion are commonly called the *stationary points*. A Taylor expansion around these points substituted into the integral (4.21), yields approximative solutions of the form,

$$\int_{-\infty}^{\infty} f(x)\mathrm{e}^{\mathrm{i}g(x)}\mathrm{d}x \approx f(x_s)\mathrm{e}^{\mathrm{i}g(x_s)}\int_{-\infty}^{\infty}\mathrm{e}^{\mathrm{i}g''(x_s)(x-x_s)}\mathrm{d}x = f(x_s)\mathrm{e}^{\mathrm{i}g(x_s)}\sqrt{\frac{2\pi}{\mathrm{i}g''(x_s)}}. \tag{4.22}$$

When we apply his method to the k_χ-integrals ($\chi = x,y,z$) in the expectation value, Eq. (4.20), the stationary points read,

$$k_\chi^s = -\frac{\tilde{A}_\chi + (R_{j_\chi} - R_{j'_\chi})}{t-t'} \tag{4.23}$$

and $g''(k_\chi^s) = -(t-t')$. The SPM generally yields HHG spectra that are completely consistent with the harmonics obtained from exact integrations of the momentum integrals. Nevertheless, the SPM has a fundamental issue when considering HHG in graphene; The antisymmetry of the p_z orbitals, combined with an external field polarized in the molecular plane such that the stationary points $k_z^s = 0$, result in vanishing spatial integrals. Thus for in-plane polarized fields the momentum integrals must be evaluated analytically.

4.3.3 Exact integration

The convenient form of the GTOs makes the analytical evaluation of the integrals needed for the HHG spectrum rather straightforward. For the spatial integrals $R(\mathbf{k},t')$ and $\mathbf{V}(\mathbf{k},t)$, as well as for the momentum integrals, the problem reduces to integrals of the form [59]

$$\begin{aligned} F_n^{\pm}(\beta,u) &= \int_{-\infty}^{\infty}\mathrm{e}^{\pm\mathrm{i}uv}v^n\mathrm{e}^{-\beta v^2}\mathrm{d}v \\ &= (\pm\mathrm{i})^n\sqrt{\frac{\pi}{\beta}}\frac{n!}{2^n\beta^{n/2}}\mathrm{e}^{-u^2/4\beta}\sum_{k=0}^{[n/2]}\frac{(-1)^k}{k!(n-2k)!}\left(\frac{u}{\sqrt{\beta}}\right)^{n-2k}. \end{aligned} \tag{4.24}$$

The expectation value of the momentum operator, Eq. (4.12), can neatly be expressed as

$$\begin{aligned} &\langle\Psi(\mathbf{r},t)|\mathbf{p}|\Psi(\mathbf{r},t)\rangle^{\mathrm{SFA}} \\ &\quad\approx -2\mathrm{Re}\left[\frac{\mathrm{i}}{(2\alpha)^5 N}\int_0^t \mathrm{e}^{\mathrm{i}\left[\varepsilon_0(t-t')-\frac{1}{2}\int_{t'}^t \mathbf{A}^2(t'')\mathrm{d}t''\right]}\right. \\ &\qquad\left.\times\sum_{j,j'}\begin{pmatrix} \mathcal{F}_{2,0,2} & \mathcal{F}_{1,1,2} & \mathcal{F}_{1,0,3} \\ \mathcal{F}_{1,1,2} & \mathcal{F}_{0,2,2} & \mathcal{F}_{0,1,3} \\ \mathcal{F}_{1,0,3} & \mathcal{F}_{0,1,3} & \mathcal{F}_{0,0,4}\end{pmatrix}\cdot\mathbf{A}(t')\mathrm{d}t'\right], \end{aligned} \tag{4.25}$$

where we have used the contracted notation denoted by

$$\mathcal{F}_{k,l,m} = F_k^+\left(\tau, \sigma_x^{j,j'}\right) F_l^+\left(\tau, \sigma_y^{j,j'}\right) F_m^+\left(\tau, \sigma_z^{j,j'}\right), \tag{4.26}$$

with $\tau = [1/\alpha + \mathrm{i}(t-t')]/2$ and $\sigma^{j,j'} = \mathbf{R}_j - \mathbf{R}_{j'} + \int_{t'}^{t} \mathbf{A}(t'')\mathrm{d}t''$.

The above integration methods, SPM and exact evaluation, allow for calculations of harmonic generation in graphene for linearly as well as circularly polarized fields with arbitrary polarization angles. The results presented in Paper IV and V indicate that graphene may indeed be a promising material for such non-linear optical processes.

CHAPTER 5

INTRODUCTION TO THE PAPERS

Paper I: *Interatom intrashell blockade*

In this paper we explore the interaction dynamics of two initially excited Rydberg atoms. The atoms are placed in a static electric field in the z direction, which splits the energy levels, according to the linear Stark effect. A weak time-dependent microwave field drives transitions between the initial circular Stark state and the most polarized, or linear, state. Isolated, such atomic intrashell transitions can be driven between the initial and final states with almost unit probability. For two interacting Rydberg atoms, however, the strong dipole-dipole interaction induces a conditional behavior of the intrashell dynamics. We identify three characteristic regimes depending on the interatomic separation R; A conditional regime, where the atoms exhibit entangled conditional behavior, is separated to the region in which the atoms behave independently by a conditional radius, R_c. The innermost region, separated from the conditional region by a blocking radius, R_b, is where the atoms are completely locked in their initial states, and no intrashell transitions occur. This controllable conditional behavior makes Rydberg atoms an interesting and promising candidate within quantum information.

In the making of this paper I contributed in the development of the code, mostly debugging and performing some of the calculations. I also contributed to the making of the figures.

Paper II: *Long-range interaction and state characteristics of interacting Rydberg atoms*

In this paper we investigate the long-range interaction between mutually excited Rydberg atoms in principal quantum numbers $n = 4, 8, 16$. The quasimolecular states are constructed from the basis of hydrogen-like product states with the configuration interaction method and with the inclusion of all order multipole moments of the total electrostatic interaction. We found that the energy curves are both attractive and repulsive, generally non-intersecting and the repulsion splitting is stronger than the attractive. The electronic probability densities of the selected states are studied as well as their relation to the single product states consisting of linear Stark states on each atom. One of the observed features is that the least bound states are always characterized by

a high degree of polarization favored towards the molecular center, and therefore well approximated by a product of two Stark states. The most bound states are similarly expressed as a coherent combination of such states which secure symmetry with respect to electron exchange and parity.

I contributed to the development and running of the code used to perform calculations for this paper, and I made some of the figures. I also participated in the writing of the paper.

This paper was picked up by the Editorial Board of Journal of Physics B to feature within the "Highlights 2011" collection.

Paper III: *Femtosecond-pulse-train ionization of Rydberg wave packets*

This paper is a study of the dynamics of a Rydberg wave packet in the principal $n = 16$ shell subjected to a train of femtosecond laser pulses. The Rydberg wave packet is placed in a microwave setup that drives transitions periodically between the initial circular state and the linear state. We use first-order perturbation theory to calculate the ionization probability as function of the number of succeeding pulses and repetition rate. We also study the angular distribution of the ionized wave packet. The total ionization probability is shown to depend crucially on the laser repetition rate, originating in the strong dependency of the ionization probability on the Stark quantum number k of the initial state.

The computer code used in this paper, as well as the main parts of the theory behind it, has been developed by myself in close collaboration with the second author. I performed calculations, wrote parts of the paper, and made some of the figures.

Paper IV: *High-order harmonic generation from graphene: Strong attosecond pulses with arbitrary polarization*

In this paper we explore high-order harmonic generation (HHG) from a graphene sheet irradiated by an intense linearly polarized femtosecond laser pulse within the Lewenstein model. The bound wavefunction of the graphene sheet is described as a coherent sum of Gaussian type p_z orbitals distributed on a two-dimensional hexagonal (honeycomb) lattice. We present results showing that the HHG cutoff frequency increases with graphene size up to the classical limit for interactions with linearly polarized laser fields. In addition we found that the extended nature of graphene allows for a strong HHG signal at maximum cutoff, and in contrast to diatomic molecules the cutoff frequency in graphene remains constant even if the diameter of the sheet extends beyond the maximal electron excursion.

I developed the theory and codes employed in this paper together with the coauthors. I participated in all parts of the writing process, including the making of the figures.

Paper V: *High-order harmonic generation in graphene flakes exposed to circularly polarized femtosecond pulses*

In Paper IV we employed the stationary phase method in the calculations of high-order harmonics from a graphene sheet. We experienced that this method fails when combining the p_z orbitals representing graphene and certain orientations of the polarization vector of the incident laser field. Therefore, in this paper we study the high-order harmonic generation from graphene by exact evaluations of the momentum integrals. The incident laser field is circularly polarized, and the plane of polarization is tilted with respect to the molecular plane. We found that both the cutoff frequency and the general structure of the harmonic spectra depend strongly on the tilt angle. Additionally, we observed exaggerated cutoff frequencies as compared to the classical limit. Whether these results really represent a characteristic feature of HHG in graphene is left as an open question. Nevertheless, the stable lattice structure makes graphene a promising material for the generation of high-energy photon pulses.

The codes used in this paper are modified from the codes utilized in Paper IV, and I have been partly responsible for the modifications. I contributed to all parts of the making of the paper.

CHAPTER 6

SUMMARY AND OUTLOOK

The work presented in this dissertation ranges from single Rydberg atoms interacting with weak fields, to diatomic Rydberg molecules and extended molecular systems irradiated by intense lasers. Nevertheless, a common feature of these systems is their extended nature as compared to ground state atoms, and the emphasis has been on the electrons' response to external fields.

We found that in the asymptotic regime of interacting Rydberg atoms the strong dipole-dipole interaction induces a shift in the energy levels that leads to a significant dependency of both the *intershell* and the *intrashell* excitation on the separation between the atoms. Results in this work point to that controlled transitions can be made between the attractive and the repulsive energy states, and thus serve as a way to handle the constant interplay between Rydberg atoms in cold gases to avoid unwanted heating and ionization. The stabilization of Rydberg matter is a prerequisite for the controlled manipulations of interacting Rydberg atoms. During the last forty years the entangled behavior of such atoms have been studied extensively, and in 2012 Serge Haroche and David J. Wineland shared the Nobel Prize in Physics for the invention of methods for measuring and manipulating individual quantum states [60]. Haroche's group used prepared circular Rydberg states in a microwave cavity to control and measure photons without destroying the photon's initial state. It is not unlikely that such a setup in the future may serve as a device for measurement and manipulation of more complex structures with a wide range of potential applications. The cavity quantum electrodynamic combined with laser cooling and trapping techniques has proposed applications in quantum optics and quantum information [61], and the conditional behavior of Rydberg atoms makes them interesting candidates for the realization of quantum bits for implementations in quantum computers [19].

The study of high-order harmonic generation of graphene reveals that graphene is indeed an interesting material for non-linear optical processes in nanosystems. The solid grid structure of graphene allows for a large number of potential recombination sites, which opens for generation of strong high-order harmonics and selective harmonic generation. In contrast to diatomic molecules, HHG in graphene provides a maximum cutoff frequency with a high yield even when the graphene molecule extends beyond the classical limit. The possibility to have strong attosecond pulse generators as table top devices allows us to carry out electronic orbital reconstructions with Ångström resolution, and opens for the enhanced imaging of ultrafast atomic and molecular dynamics. Such devices are powerful tools in the quest for understanding

the electronic orbital structure in molecular and solid structures as well as the dynamics in external electromagnetic fields. To reach this level it is called for experiments to probe these phenomena and further theoretical research should develop more realistic and applicable electronic models of the graphene flakes. The capability to monitor and govern chemical and physical properties is a prerequisite for the control of nanosystems utilized in areas as distant as material science, renewable energy production and medical diagnostics and treatment. However, independent of potential applications it is a subject of fundamental interest in its own right.

CHAPTER 7

SCIENTIFIC RESULTS